A meso-mechanical model of the tensile behaviour of concrete. Part II: modelling of post-peak tension softening behaviour

J. HUANG and V. C. LI

(Massachusetts Institute of Technology, USA)

An analytic constitutive model is derived for the post-peak behaviour of composite concrete. Tension softening is modelled in relation to propagation of a dominant crack against an effective toughness which accounts for crack deflection and the existence of distributed interfacial cracks. Analytic expressions for the tension softening curve and fracture energy are derived in terms of internal material parameters. Limited comparison between model predictions and experimental data and an overall discussion of the effects of internal material parameters on composites properties are presented.

Key words: *concrete; tension; tension–softening relation; critical separation; fracture energy; aggregate pull-out; aggregate volume fraction; aggregate size; w/c ratio*

The post-peak tension–softening behaviour of concrete has been studied by many researchers.[1–5] Horii *et al*[6] modelled the tension–softening curve by considering concrete in the post-peak stage as an idealized body containing a periodic array of microcracks with identical crack length and spacing. By using known stress intensity factor at the microcrack tips, the ambient tensile load is related to the crack length and thus, related to the average separation.

In the present paper a simple tension–softening relation is developed by using linear-elastic fracture mechanics on the meso-scale. The post-peak behaviour is modelled as an extension of the largest crack, called dominant crack. (In Part I, the development of the cement/aggregate interface crack in relation to distributed inelastic deformation was described. The branching of the largest crack from the cement/aggregate interface into the matrix is assumed to be associated with the tensile strength).

DOMINANT CRACK PROPAGATION

After the peak load is reached, the dominant crack propagates unstably, whereas other smaller cracks become inactive. The dominant crack may be simplified approximately as one that is straight, with crack length equal to $2(L + R_{max})$, where L is the length of crack in the cement matrix. If the presence of other aggregates is not considered, the propagation of a straight crack within the matrix is governed by the equation

$$\sigma\sqrt{\pi(L + R_{max})} = K_{Ic}^{m} \quad (1)$$

where K_{Ic}^{m} is the cement matrix toughness.

The fracture path is generally tortuous in normal concrete, in contrast to plain cement paste in which the fracture path is rather planar. The tortuosity of the fracture path may be related to the crack deflection effect. When the dominant crack intercepts another aggregate, it would most likely deflect around the aggregate because the cement/aggregate interface is weak.[7] Deflection reduces the stress intensity factor at the new tip because the deflected crack tip orientation is no longer perpendicular to the applied load. Effectively, the material is toughened.

In addition to crack deflection toughening, the presence of cracks at cement/aggregate interfaces increases the material's toughness. The interfacial cracks reduce the elastic modulus of the material ahead of the dominant crack, lowering the stress intensity

0010-4361/89/040370-09 $3.00

factor at the dominant crack tip and providing a shielding effect. Again, the material is effectively toughened.

To account for the above fracture processes, it is envisaged that the dominant crack propagates into a homogeneous material with an effective toughness K_{Ic}^{eff} higher than K_{Ic}^{m}. The toughening mechanisms and the resulting K_{Ic}^{eff} are discussed in the following paragraphs. It should be noted that other toughening and damaging mechanisms not accounted for in the present modelling effort may be operational simultaneously. These include, for example, crack blunting when it runs into an air void, or discontinuous crack planes (branching) which subsequently link, and which increase the fracture surface area.

TOUGHENING MECHANISMS

Crack deflection toughening

To evaluate crack deflection toughening, it is necessary to examine the reduction in crack-tip stress intensity for different deflection angles, illustrated in the inset of Fig. 1. This problem was solved by Faber *et al.*[8] Extension of the deflected portion of the crack was considered to be governed by the requirement that the strain energy release rate G attains the critical value G_c, related to the matrix toughness K_{Ic}^{m}. The strain energy release rate, averaged over all possible deflecting angles, was calculated by using a probabilistic analysis:

$$K_{Ic}^{def}/K_{Ic}^{m} = \sqrt{1.0 + 0.87\,V_f} \qquad (2)$$

where K_{Ic}^{def} is the effective toughness due to crack deflection. The volume fraction of inclusions, V_f, comes into the equation through the consideration of the probability of crack-aggregate interceptions. For V_f = 0.1, 0.3, 0.5 and 0.7 K_{Ic}^{def}/K_{Ic}^{m} = 1.04, 1.12, 1.20 and 1.27 respectively, Fig. 1. The possibility that the propagating crack does not intersect the centre of the aggregate has also been considered in the derivation of Equation (2).

Toughening due to distributed interfacial cracks

The formation and propagation of a dominant crack implies a stress relaxation and possibly closure of

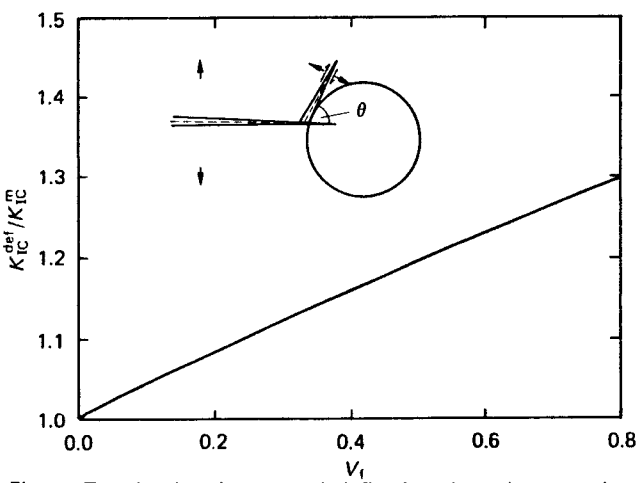

Fig. 1 Toughening due to crack deflection about the second phase inclusion at angle θ

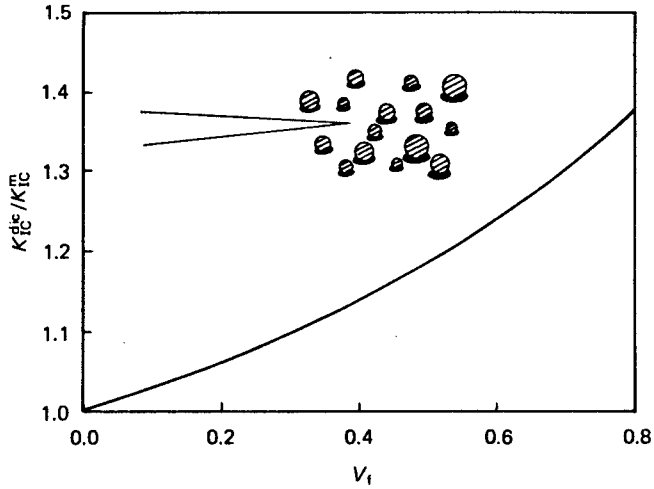

Fig. 2 Toughening due to the interfacial cracks ahead of the dominant crack and schematic diagram indicating shielding effect

interfacial cracks in the material away from the dominant crack. This material may be expected to unload elastically with an elastic modulus similar to the uncracked state. However, in the zone of material ahead of the dominant crack, the high tensile stress there would keep the interfacial cracks open, resulting in a material with Young's modulus effectively smaller than the original uncracked material. By considering the path independence of the J-integral, Evans and Faber[9] showed that the dominant crack tip stress intensity factor is lowered by the reduced local modulus, resulting in a toughening effect. Hence

$$K_{Ic}^{dic}/K_{Ic}^{m} = \sqrt{E_m\,(1 - \nu)/E\,(1 - \nu_m)} \qquad (3)$$

where K_{Ic}^{dic} is the material toughness with distributed interfacial cracks, E_m is Young's modulus for the material devoid of cracks, E is the modulus with interfacial cracks, and ν and ν_m are the corresponding Poisson's ratios.

By using the self-consistent technique employed by Budiansky and O'Connell[10] in treating the distributed interfacial cracked body, and assuming that each aggregate has one interfacial crack, the reduced elastic moduli may be related to the volume fraction of aggregates by

$$\frac{E}{E_m} = 1 - \frac{\pi^2}{16}(1 - \nu^2)\,V_f \qquad (4)$$

Details of the derivation are given in Appendix A.

Substitution of Equation (4) into (3), assuming $\nu = \nu_m$, results in the toughness increase

$$K_{Ic}^{dic}/K_{IC}^{m} = \sqrt{\frac{1}{1 - (\pi^2/16)\,V_f\,(1 - \nu^2)}} \qquad (5)$$

For ν = 0.20 and V_f = 0.1, 0.3, 0.5 and 0.7 and K_{Ic}^{dic}/K_{Ic}^{m} = 1.03, 1.10, 1.19 and 1.30 (Fig. 2)

Effective toughness

Taking into account the crack deflection and interfacial cracking effects, and assuming that these two

mechanisms operate independently, the effective toughness of the material can be written as

$$K_{Ic}^{eff}/K_{Ic}^{m} = \sqrt{1.0 + 0.87\,V_f}\sqrt{\frac{1}{1 - (\pi^2/16)\,V_f(1 - \nu^2)}} \quad (6)$$

For $\nu = 0.20$, $V_f = 0.1, 0.3, 0.5$ and 0.7 and $K_{Ic}^{eff}/K_{Ic}^{m} = 1.07, 1.24, 1.43$ and 1.66. This implies that the dominant crack propagates into a 'homogeneous' material whose toughness is 66% higher than the cement matrix toughness, for a concrete with $V_f = 0.7$.

Equation (6) is also used in calculating the concrete tensile strength, f_t, in part I, which gives

$$f_t\sqrt{\pi R_{max}} = K_{Ic}^{eff} \quad (7)$$

Here, for simplicity, the effect of crack interactions discussed in part I is assumed to be negligible. The matrix toughness in Equation (1) should now be replaced by the effective toughness as

$$\sigma\sqrt{\pi(L + R_{max})} = K_{Ic}^{eff} \quad (8)$$

TENSION–SOFTENING RELATION

Calculation of tension–softening curves

To calculate the tension–softening curve, the relationship between the ambient tensile stress, σ, and the opening separation, δ, on the failure plane must be determined. The progressive formation of this failure plane is probably associated with the expansion of the dominant crack, and δ is equated with the average opening contribution of this crack. Thus δ increases as the crack expands against the effective fracture toughness K_{Ic}^{eff} given by Equation (6). In relating δ to the crack length L in Equation (8), carried out in detail in Appendix B, it is assumed that the crack length jumps by the size of the aggregate each time the dominant crack intercepts an aggregate. This phenomenon contributes to a larger δ at a given load σ, which is accounted for approximately by modifying the crack length L with respect to aggregate volume fraction V_f in the present modelling. Details of this modification are also presented in Appendix B. The resulting tension–softening curve, relating δ and σ, is

$$\delta = \frac{(K_{Ic}^{eff})^2(1 - \nu^2)}{E(1 - V_f)f_t}\,\frac{1}{(\sigma/f_t)}\,[1 - (\sigma/f_t)^3] \quad (9)$$

Equation (9) shows the post-peak behaviour dependence on the Young's modulus, E, the Poisson's ratio, ν, the aggregate volume fraction, V_f, the tensile strength, f_t, and the matrix toughness, K_{Ic}^{m} (implicitly expressed in K_{Ic}^{eff}). It is interesting to note that the cement/aggregate interfacial toughness affects the σ–δ curve only through f_t.

The tension–softening curve predicted by the present model is plotted in Fig. 3 for some typical values of the material parameters of concrete. The stress drops sharply with a long tail, with the initial slope strongly controlled by the ratio $(K_{Ic}^{eff})^2/Ef_t$. The area under the curve represents the energy release rate G_c of the composite.

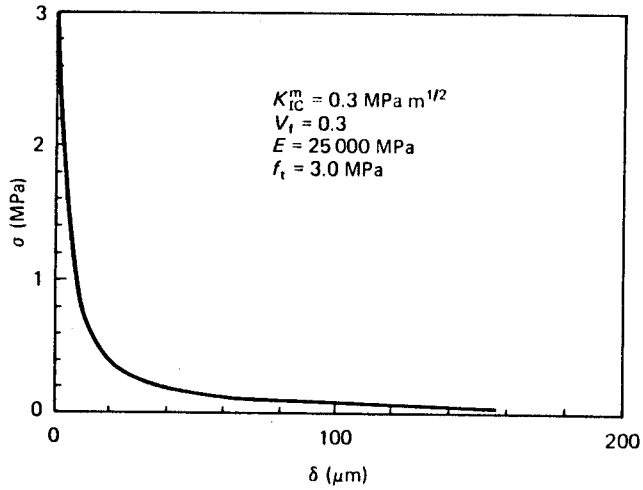

Fig. 3 The predicted tension–softening curve for a typical concrete

Comparison of theoretical and experimental results

Comparison of the predicted tension–softening relations with the experimental results given by Refs 1 and 2 is illustrated in Fig. 4(a) and 4(b). In both Refs 1 and 2, the matrix toughness K_{Ic}^{m} was not given, so the curves were plotted for a range of typical K_{Ic}^{m} values of concrete. The critical separation δ_c, which is used to normalize the separation δ, is taken to have the same value as that which is given by the experimental data. (In Ref. 2, the critical separation δ_c was obtained only

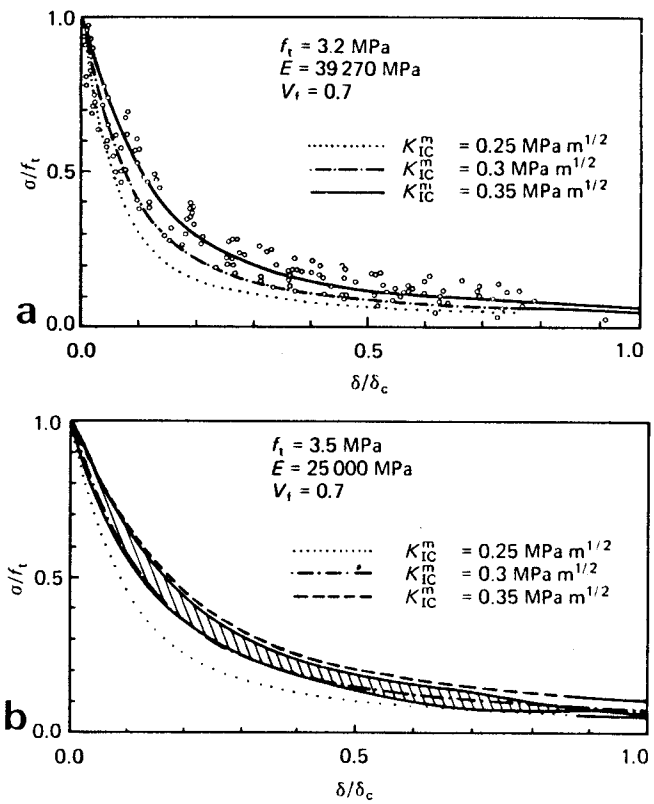

Fig. 4 (a) comparison of predicted and measured normalized tension–softening curve. The aggregate and sand specific density is assumed to be 2.6, and cement specific density 3.15, approximately, in the calculation of V_f. The experimental data is from Ref 1, and (b) comparison of predicted and measured normalized tension–softening curve. The experimental data (shaded area) is from Ref. 2

for one of four tests). The experimentally determined δ_c is usually obtained by measuring the opening separation of the failure plane at the moment when the stress reduces to zero. The determination of the critical separation in the new model will be discussed. The tension–softening curve predicted compares reasonably well with the experimental data.

Determination of critical separation

In the final stages of a uniaxial tensile failure, a macroscopic fracture plane forms through the cross-section of the specimen. The coarse aggregate particles are subsequently extracted from either face of the fracture plane. The frictional pull-out of the aggregate is thought to be the most important failure mechanism at this stage by many authors.[1,2] The assumption that the σ–δ curve is controlled by a crack-like deformation mode is no longer valid. Instead, the frictional force which supplies the stress-transferring capacity across the failure plane has to be considered.

Unlike fibre pull-out, in which the critical separation of the failure plane is just equal to half the length of the fibre, the critical separation in aggregate pull-out is much smaller than the aggregate radius, as shown by many experiments.[1–3] To describe the aggregate pull-out process, parameter, η, defined as a measurement of the roughness of the aggregate surface is introduced. When an aggregate is being pulled out from the cement matrix, interlocking of the matrix and aggregate, through roughness η, supplies the resistance to the separation of the plane. This resistance reduces to zero only when the matrix and aggregate can shear through freely, when there will be no resistance to the further opening of the failure plane, Fig. 5. By geometric analysis, assuming the maximum aggregate is the last one to be pulled out, the critical separation is obtained as

$$\delta = \sqrt{2R_{max}\,\eta} \tag{10}$$

Frictional pull-out of aggregates

The aggregate pull-out can now be studied by taking a unit cell from the failure plane, Fig. 6. Assumptions are that: the cement matrix is very brittle so the load is carried by the frictional force at interfaces only; and

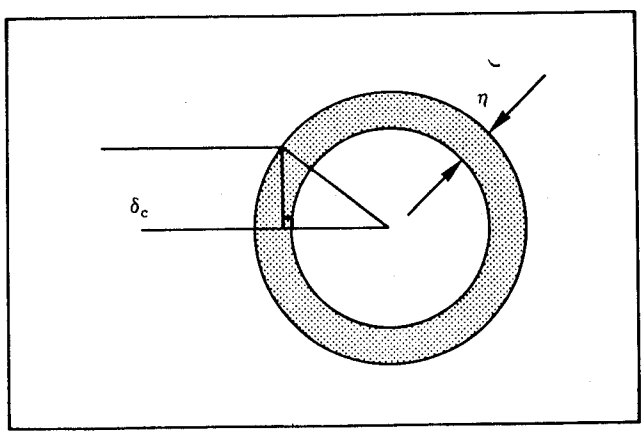

Fig. 5 An aggregate with roughness η

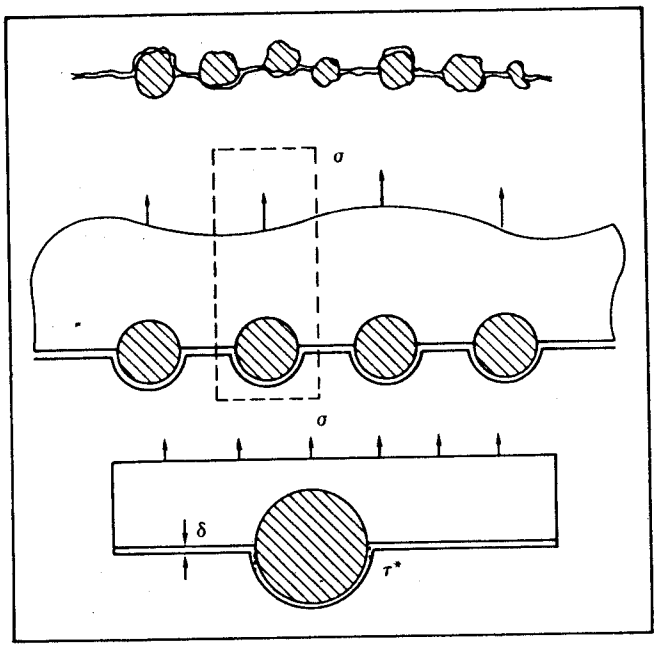

Fig. 6 Schematic diagram of aggregate frictional pull-out and a unit cell of the failure plane

each aggregate has an average radius R_{avg}. The equilibrium of the unit cell requires

$$\sigma\,(2R_{avg}/V_f) = \tau^*(\delta_c - \delta) \tag{11}$$

where σ is tensile stress and τ^* is the interfacial shear strength.

The average aggregate radius, R_{avg}, can be taken as the mean value of the random size distribution. For the Fuller-curve distribution

$$R_{avg} = \int_0^{R_{max}} rf(r)\,dr = (1/3)R_{max} \tag{12}$$

Substituting Equation (12) into (11), the tension–softening curve in the stage of final failure is obtained

$$\sigma = (3V_f/2R_{max})\,\tau^*\,(\delta_c - \delta) \tag{13}$$

or in the non-dimensional form

$$\frac{\sigma}{f_t} = \frac{3V_f}{2R_{max}}\,\delta_c\,\frac{\tau^*}{f_t}\left(1 - \frac{\delta}{\delta_c}\right) \tag{14}$$

The stress σ is linearly dependent on the separation.

Fig. 7 shows a complete tension–softening relation. At the initial stage, when the crack separation is small, the material is characterized by the behaviour of a dominant crack. In the final stage of failure, the frictional pull-out becomes dominant. The strength decay rate (Fig. 7) is affected by the ratio between the material parameters τ^* and f_t. The exact value of τ^*/f_t, and the roughness parameter η which controls δ_c, need to be determined experimentally.

Energy release rate G_c

The area under the tension–softening curve represents the energy release rate, G_c, of the composite concrete.

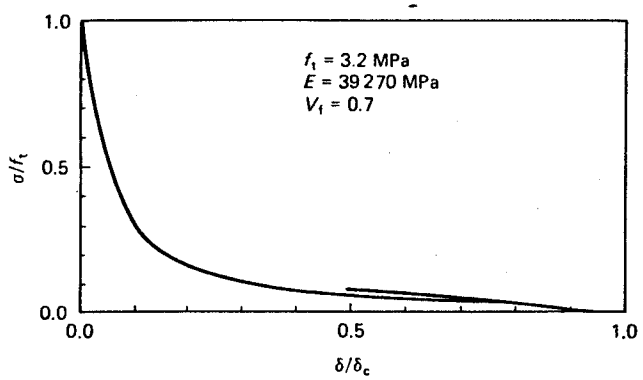

Fig. 7 A complete tension–softening curve

Although there are two regions, one corresponding to the dominant crack propagation part, the other corresponding to the frictional pull-out part, only the tension–softening relation in the first region is used to calculate G_c. The error due to this approximation is expected to be small because the frictional pull-out functions only near the very end stage of failure. Integrating over the area until $\delta = \delta_c$ gives

$$G_c = \int_{\sigma_c}^{f_t} \left\{ \frac{(K_{Ic}^{eff})^2 (1 - \nu^2)}{E (1 - V_f) f_t} \frac{1}{(\sigma/f_t)} [1 - (\sigma/f_t)^3] \right\} d\sigma + \sigma_c \delta_c \quad (15)$$

where σ_c is the stress corresponding to $\delta = \delta_c$ in the first region. Simplifying Equation (15) results in

$$G_c = \delta_c f_t [(2/3) t_c - \beta \ln t_c] \quad (16)$$

where

$$t_c = \frac{\sigma_c}{f_t}$$

$$\beta = \frac{[(K_{Ic}^{eff})^2 (1 - \nu^2)]}{[\delta_c f_t E (1 - V_f)]} \quad (17)$$

with

$$\delta_c = \sqrt{2 R_{max} \eta}$$

$$f_t = \frac{K_{Ic}^{eff}}{\sqrt{\pi R_{max}}} \quad (18)$$

DISCUSSION

There are several ways to produce concrete with higher strength, *eg* reducing water cement (w/c) ratio, adding silica fume admixture and/or using small crushed aggregates. Although high strength usually means high compressive strength, most factors affecting compressive strength have the same effects on tensile strength. Using small-size aggregate reduces the size of bond cracks and the initial dominant crack size. The addition of silica fume in combination with a superplasticizer can lead to reduced water demand, densified cement paste and stronger bondings. The resulting high strength concrete is characterized by a fine pore size distribution and a densification of the paste matrix microstructure in the cement/aggregate interface zone. The reduced porosity also leads to a high cement matrix toughness.[16] Factors controlling strength and toughness of concrete are analysed in th light of the theoretical model introduced in the previous sections.

Effect of aggregate size on composite properties

The tensile strength decreases with the maximum aggregate size R_{max} as indicated by Equation (7). Equations (6) and (7) also imply an increase of tensil strength with volume fraction of aggregate, other thi being equal. In normal concrete design, however, th aggregate volume fraction and the maximum aggrega size are not independent variables. The amount of aggregate varies with the maximum aggregate size in order to maintain reasonable workability. Based on t mix design code given by Ref. 11, the predicted changes in tensile strength f_t with maximum aggrega size D_{max}($= 2R_{max}$) is shown in Fig. 8(a). Following the same mix design code and using Equation (16), th critical energy release rate, G_c, is calculated and plotted in Fig. 8(b). These figures suggest that while reducing the maximum aggregate size improves the tensile strength, there is also a simultaneous trade of the fracture toughness of the material.

Limited experimental data on the variation of the critical energy release rate G_c of normal concrete for

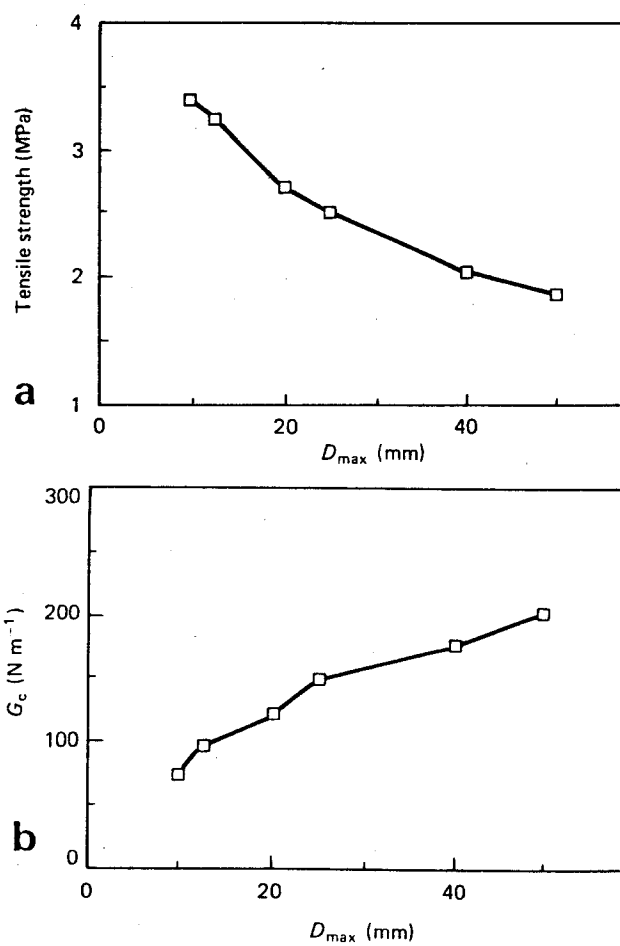

Fig. 8 (a) model predicted tensile strength and (b) model predicted critical energy release rate, shown as a function of maximum aggregate size

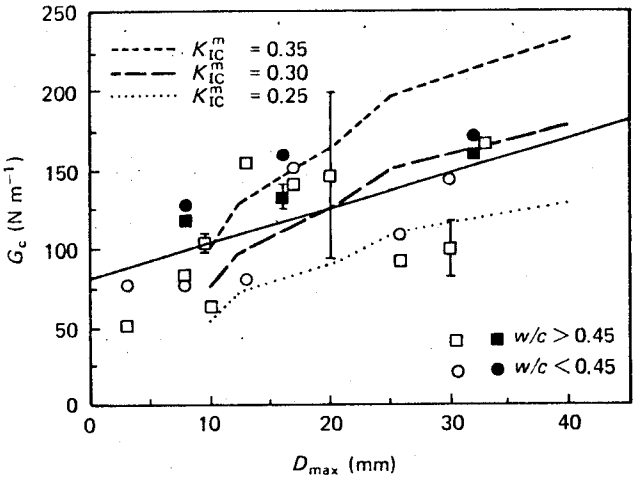

Fig. 9 Comparison of predicted and measured critical energy release rate as a function of maximum aggregate size. The experimental data is from Ref. 12

various maximum aggregate sizes has been reported,[12] using two concrete materials with different water/cement ratios. Additional recent data can be found.[17] The combined data set, shown in Fig. 9, has significant amount of scatter, even though the general trend (indicated by the solid linear regression line for all experimental data points) is consistent with the trends predicted by the present model. The model predicted trends in Fig. 9 are based on the same mix design code mentioned and for three different cement matrix toughnesses. The experimental data from Ref. 12 was obtained from equal sized notched beams based on the RILEM recommended G_F fracture test.

It should be pointed out that the trade-off between tensile strength and fracture energy with maximum aggregate size discussed is meant to describe the behaviour of normal concrete only. For high strength concrete, the addition of superplasticizer greatly enhances workability. This leads to a closer packing of cement grains and to a rise of the cement matrix and possibly the concrete toughness.

Effect of interfacial and matrix toughness on composite behaviour

The reduction of porosity and large pore size in cement paste as well as the densification of the interfacial zone can be expressed in terms of an increase in cement matrix toughness, K_{Ic}^m; and interfacial toughness, K_{Ic}^{if}. Their effects on concrete tensile strength could be predicted by the present model.

In the previous calculation, the ratio $K_{Ic}^{if}/K_{Ic}^m = 0.6$ was used, which implies a regular bonding for normal concrete. For better interfacial bondings, *ie* $0.6 < K_{Ic}^{if}/K_{Ic}^m < 1.0$ (note that $K_{Ic}^{if} < K_{Ic}^m < K_{Ic}^{agg}$ is always assumed in the present model) the crack at the largest aggregate interface would branch into the matrix at an angle less than $\pi/2$. The relation between the stress and the crack length after branching has the following form

$$\sigma\sqrt{\pi(L + R_{max}\sin\theta)} = \alpha K_{Ic}^m \qquad (19)$$

where $\alpha = K_{Ic}^{eff}/K_{Ic}^m$

Table 1 Values for branching angle, toughening effect and tensile strength for $V_f = 0.3$ where $f_t^o = f_t\sqrt{R_{max}/K_{Ic}^m}$

θ^*	50°	60°	70°	80°	90°
K_{Ic}^{if}/K_{Ic}^m	1.01	0.92	0.81	0.72	0.65
f_t^o	0.793	0.746	0.716	0.699	0.694

Again, assuming $\sigma = f_t$, when the first branching occurs, Equation (19), together with Equation (2) in part I, can be used to solve two unknowns, tensile strength f_t and branching angle θ^*. This gives

$$\frac{K_{Ic}^{if}}{K_{Ic}^m} = \frac{\alpha}{\sqrt{\pi}} \frac{1}{F(\theta^*)\sqrt{\sin\theta^*}}$$

$$\frac{f_t\sqrt{R_{max}}}{K_{Ic}^m} = \frac{\alpha}{\sqrt{\pi\sin\theta^*}} \qquad (20)$$

Values of θ^*, K_{Ic}^{if}/K_{Ic}^m and f_t^o are shown in Table 1 where $f_t^o = f_t\sqrt{R_{max}/K_{Ic}^m}$.

Within the range $K_{Ic}^{if} \leq K_{Ic}^m$, the smallest branching angle θ^* equals 50°. Thus according to the model, in going from regular bond, $K_{Ic}^{if}/K_{Ic}^m = 0.65$, to good bond, $K_{Ic}^{if}/K_{Ic}^m = 1.0$, tensile strength increases by about 14.3%. This result is consistent with the observation of Mindess[13] 'Most studies of strength, be they tensile, compressive, or flexual, have shown that improving the cement aggregate bond strength does increase the concrete strength, but the effect tends to be moderate. In going from little or no bond to the best bond that can be achieved, strengths have been observed to increase by about 20–40%.'

Equation (20) also indicates that concrete tensile strength is proportional to the cement matrix toughness K_{Ic}^m. This implies that a change in matrix toughness has more effect on concrete strength than a change in interfacial toughness. Although quantitative comparison with experimental data is not possible because most data were reported in terms of matrix or interfacial strength instead of toughness, it is still possible to get some qualitative comparisons, *eg* the paste strength is about twice as important as the bond strength in determining the concrete strength.[13,14]

A relationship between tensile strength and *w/c* ratio was reported by Zielinski,[15] after standardization and extrapolation of the experimental results, Fig. 10. Tensile strength decreases with increasing water/cement ratio because a higher water/cement ratio produces larger pore size, higher porosity and weaker cement/aggregate interfaces. The dots in Fig. 10 are the values predicted by the present model using K_{Ic}^m values referenced by the same paper,[15] Fig. 11. In the calculation, the change of K_{Ic}^{if}/K_{Ic}^m was not included due to the lack of experimental data of how K_{Ic}^{if} changes with *w/c* ratio, and because of the moderate effect as indicated by the discussion above. It is expected that the induced error would be small because both K_{Ic}^{if} and K_{Ic}^m are increased with reduced *w/c* ratio, so that K_{Ic}^{if}/K_{Ic}^m remains essentially unchanged.

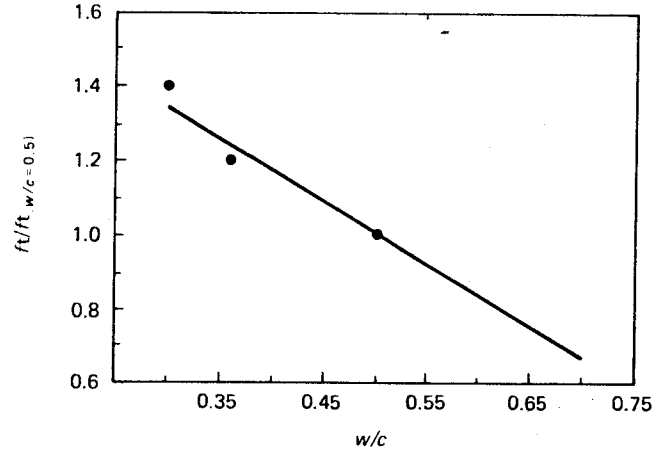

Fig. 10 Normalized tensile strength *versus* water/cement ratio

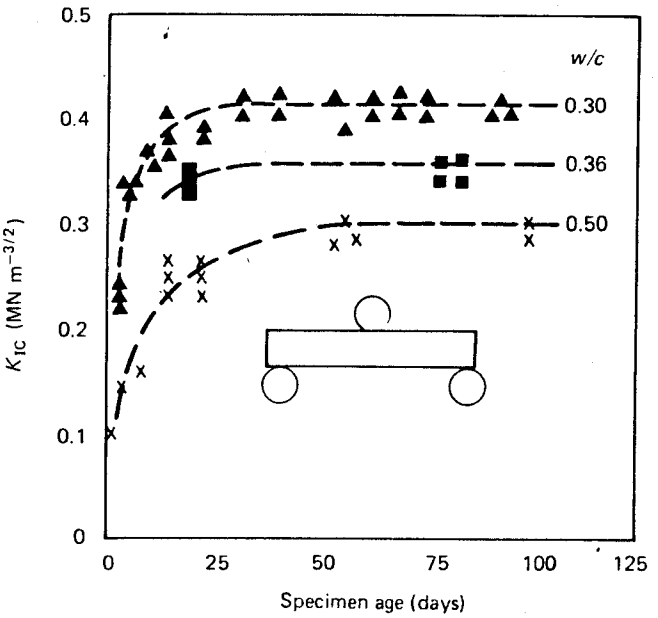

Fig. 11 Experimental measurements of cement matrix toughness K_{Ic}^{m} *versus* water/cement ratio, from Ref. 18

One limitation of the present model is that $K_{Ic}^{if} < K_{Ic}^{m} < K_{Ic}^{agg}$ is always assumed. Sometimes this assumption cannot be satisfied. For example, in high rate loading or high strength concrete with good interfacial bonds and small aggregate sizes, the cracks do not necessarily nucleate at the cement/aggregate interface, and the crack path can cut through coarse aggregate particles instead of passing around them.[16] This crack pattern implies a different failure mechanism compared with normal concrete. The toughening mechanisms accounted for in the model, such as toughening due to crack deflection or distributed interfacial cracks, will no longer exist. The present model needs to be modified before application to the problem of 'cutting through aggregate' crack pattern.

CONCLUSIONS

The macrocopic tensile behaviour of concrete is analysed by means of investigating its internal structure and failure mechanisms. In particular, a post-peak tension–softening relation is developed. The model predicts the dependencies of post-peak tension–softening relation and fracture toughness on R_{max}, V_f, and K_{Ic}^{m}. Comparisons of model predicted values with experimental data, whenever available, show reasonable agreements.

The behaviour of concrete in tension is complicated because of the inhomogeneity of the material. A complete description of it has not been presented here. The model can only be regarded as preliminary because of the many assumptions built into it: for example simplifying coarse aggregates as circular discs, assuming $K_{Ic}^{if} < K_{Ic}^{m} < K_{Ic}^{agg}$ (which may be violated in high strength concrete or concrete under high loading rate) and all the other assumptions concerning interfacial cracks and the dominant crack. The expansion of a simple dominant crack and the toughening of the matrix by distributed interfacial cracks are particularly contentious assumptions. In spite of the simplified assumptions, the model seems to be able to predict the gross features of tensile composite behaviour of concrete and provide some implications in concrete material engineering.

ACKNOWLEDGEMENTS

The authors would like to thank A. Hillerborg and S. Mindess for many helpful discussions. A grant from the National Science Foundation to the Massachusetts Institute of Technology is gratefully acknowledged.

REFERENCES

1 **Cornelissen, H. A. W., Hordijk, D. A. and Reinhardt, H. W.** 'Experiments and theory for the application of fracture mechanics to normal and lightweight concrete' in '*Fracture Toughness and Fracture Energy of Concrete*' (ed F. H. Wittmann) (1986) pp 565–575

2 **Petersson, P. E.** 'Crack growth and development of fracture zones in plain concrete and similar materials' *report TVBM-1006* (Division of Building Materials, Lund Institute of Technology, Sweden, 1981)

3 **Wecharatana, M.** 'Specimen size effects on non-linear fracture parameters in concrete' in '*Fracture Toughness and Fracture Energy of Concrete*' (ed F. H. Wittmann) (1986) pp 437–440

4 **Li, V. C., Chan, C. M. and Leung, C. K. Y.** 'Experimental determination of the tension-softening relations for cementitious composites' *Cem Concr Res* **17** (1987) pp 441–452

5 **Gopalaratnam, V. S. and Shah, S. P.** 'Softening response of plain concrete in direct tension' *ACI Journal* **82-27** (1985) pp 310–323

6 **Horii, H., Hasegawa, A. and Nishino, F.** 'Process zone model and influencing factors in fracture of concrete' *SEM/RILEM International Conference on Fracture of Concrete and Rock* (ed S. P. Shah/S. E. S. Swartz) (1987) pp 299–307

7 **Shah, S. P. and McGarry, F. J.** 'Griffith fracture criterion and concrete' *J Eng Mech Division* Proc ASCE (1971) pp 1663–1676

8 **Faber, K. T., Evans, A. G. and Drory, M. D.** 'A statistical analysis of crack deflection as a toughening mechanism in ceramic materials' in '*Fracture Mechanics of Ceramics*' **6** (ed R. C. Bradt *et al*) (1983) pp 77–91

9 **Evans, A. G. and Faber, K. T.** 'On the crack growth resistance of microcracking brittle materials' in '*Fracture in Ceramic Materials*' (ed A. G. Evans) (1983) pp 109–136

10 **Budiansky, B. and O'Connell, R. J.** 'Elastic moduli of a cracked solid' *Int J Solids Struc* **12** (1976) pp 81–97

11 **Neville, A. M.** *Properties of Concrete* (Pitman, 1981)

12 **Hillerborg, A.** 'Additional concrete fracture energy tests performed by 6 laboratories according to a Draft RILEM recommendation' *Report to RILEM TC50-FMC* (Division of Building Materials, Lund Institute of Technology, Sweden, 1984)

13 **Mindess, S.** 'Bonding in cementitious composites: How important is it?' *MRS Symposium Proceedings* **114** (ed S. Mindess and S. P. Shah) (1987) pp 3–10
14 **Alexander, K. M. and Taplin, J. H.** *Australian J Appl Sci* **13** (1962) pp 277–284; **15** (1964) pp 160–170
15 **Zielinski, A. J.** 'Behavior of concrete at high rates of tensile loading: A theoretical and experimental approach' *Report 5-83-5 Stevin Lab* (Delft University of Technology, The Netherlands, 1983)
16 **Kendall, K., Howard, A. J. and Birchall, J. D.** 'The relation between porosity, microstructure and strength, and the approach to advanced cement-based materials' *Phil Trans R Soc Lond* **A310** (1983) pp 139–153
17 **Mihashi, H., Nomura, N. and Wittmann, F. H.** 'Influence of Heterogeneity on fracture energy and strain softening of concrete' *MRS Symposium Volume on 'Fracture'* (ed Sakai, 1988)
18 **Higgins, D. D. and Bailey, J. E.** 'Fracture measurements, on cement paste' *J Mater Sci* **11** (1976) pp 1995–2003

AUTHORS

The authors are with the Department of Civil Engineering, Massachusetts Institute of Technology, Cambridge, MA 02139, USA.

APPENDIX A. Calculation of the reduction of Young's modulus due to interfacial cracks

The elastic moduli of concrete will be reduced near the peak tensile load due to interfacial cracks. In this appendix, an expression for the reduced Young's modulus is developed in terms of the aggregate volume fraction, V_f. This development is based on a self-consistent technique first utilized by Budiansky and O'Connell[10] in estimating moduli changes in 3-D randomly oriented flat-cracked elastic bodies

Let K_m, E_m and ν_m represent the bulk modulus, Young's modulus, and Poisson's ratio of an uncracked body, respectively. Let K, E and ν represent those of a cracked body. Using the self-consistent method, K, E and ν can be estimated by calculating the energy loss produced by a single isolated crack in an infinite medium having the effective properties of the cracked body. The simultaneous equations for the determination of K, E and ν for an arbitrary shaped crack in the 3-D case have the form[10]

$$\frac{K}{K_m} = 1 - \frac{2N\langle a^3 f(\nu)\rangle}{3(1-2\nu)}$$

$$\frac{E}{E_m} = 1 - 2N\langle a^3 (f(\nu)\cos^4\alpha + g(\nu,\beta)\sin^2\alpha\cos^2\alpha)\rangle$$

$$\frac{E}{K} = 3(1-2\nu) \qquad \text{(A1)}$$

where a is a characteristic linear crack dimension, *eg* the radius of a penny-shaped crack, N is the number of cracks per unit volume, f and g are non-dimensional shape factors that can depend on ν as well as on the crack shape, α represents the angle between an arbitrarily applied load and the normal of crack plane and β is the angle related to the crack orientation. The angle brackets in Equation (A1) denote an average.

Adaptation of Equation (A1) to the 2-D model requires using crack dimension a^2 instead of a^3 and taking $\beta = 0$ because all the interfacial cracks have the same orientation. With the assumption that crack sizes, shapes and orientations are uncorrelated, the averaged value in the angle brackets can be calculated by integrating α from 0 to 2π, which results in $\langle\cos^4\alpha\rangle = 3/8$, $\langle\sin^2\alpha\cos^2\alpha\rangle = 1/8$, and Equation (A1) then reduces to

$$\frac{K}{K_m} = 1 - \frac{2N\langle a^2\rangle f(\nu)}{3(1-2\nu)}$$

$$\frac{E}{E_m} = 1 - \frac{1}{4}N\langle a^2\rangle[3f(\nu) + g(\nu)]$$

$$\frac{E}{K} = 3(1-2\nu) \qquad \text{(A2)}$$

The shape factor $f(\nu)$ arises in considering the potential energy loss $(\Delta\psi)_p$ in the solid due to the introduction of a single crack in an infinite medium having the effective properties of the cracked bodies, and under hydrostatic load p, such that

$$(\Delta\psi)_p = \frac{p^2a^2}{E} f(\nu) \qquad \text{(A3)}$$

from dimensional analysis. For an infinite plate containing a flat crack

$$(\Delta\psi)_p = 2\int_0^a G_c\,da$$

$$G_c = \frac{p^2\pi a(1-\nu^2)}{E} \qquad \text{(A4)}$$

where G_c is the energy release rate. Integrating Equation (A4) and comparing the result with Equation (A3) gives

$$f(\nu) = \pi(1-\nu^2) \qquad \text{(A5)}$$

For the shape factor $g(\nu)$ which arises in a similar consideration of potential energy loss but under uniaxial loading, simple dimensional analysis and specialization to the 2-D case leads to

$$g(\nu) = \pi(1-\nu^2) \qquad \text{(A6)}$$

Substituting Equations (A5) and (A6) into (A2)

$$\frac{K}{K_m} = 1 - \frac{2\pi(1-\nu^2)}{3(1-2\nu)}N\langle a^2\rangle$$

$$\frac{E}{E_m} = 1 - \pi(1-\nu^2)N\langle a^2\rangle$$

$$\frac{E}{K} = 3(1-2\nu) \qquad \text{(A7)}$$

To calculate $N\langle a^2\rangle$ in Equation (A7), it is assumed that each aggregate has one interfacial crack of length $(\pi/4)R$. In reality the interfacial crack lengths probably

span a spectrum $0<\theta<\theta_2$. For a random aggregate size distribution,

$$N\langle a^2\rangle = \frac{1}{V}\int_0^{R_{max}} \left(\frac{\pi}{4}R\right)^2 p(R)\,dR = \frac{\pi}{16}V_f \quad (A8)$$

where $p(R)$ is the number density given by Equation (10) in the text.

Substituting Equation (A8) into the second equation of (A7)

$$\frac{E}{E_m} = 1 - \frac{\pi^2}{16}(1-\nu^2)V_f \quad (A9)$$

which reproduce Equation (4) in the text. It should be noted that if the crack angle θ approaches $\pi/2$, and for large enough volume fraction V_f, Equation (A9) may predict a E/E_m approaching zero or even becoming negative. Physically this implies a loss of coherence of the material as the aggregate volume fraction approaches unity and the interfacial crack density becomes very high. In this limit the self-consistent approach used in deriving Equation (A9) breaks down.

APPENDIX B. Calculation of the tension–softening curve at the initial stage

The dominant crack will join with the interfacial crack each time it intercepts an aggregate. This leads to a jump of the dominant crack length by aggregate size D $(= 2R)$. This discontinuous expansion of the crack should lead to a lower equilibrium load. However, the new crack tip resulting in joining the dominant crack with an interfacial crack may be oriented in such a way as to require additional load to reinitiate the dominant crack. For simplicity, it is assumed that these opposing effects cancel each other out, so that the dominant crack jumps occur at essentially constant remote loads. The dominant crack jump effect is accounted for approximately in the present model using a modified crack length in calculating the opening separation.

Assuming that each aggregate has an average diameter D_{avg} and the spacing between aggregates is b, the propagation of the dominant crack is governed by the equation

$$\sigma\sqrt{\pi a} = K_{Ic}^{eff} \quad (B1)$$

where a is the total crack length, including the crack length before branching, R_{max}, and the crack length in the matrix, L.

At the peak load, when $a = R_{max}$

$$f_t\sqrt{\pi R_{max}} = K_{Ic}^{eff} \quad (B2)$$

Let a_{eff} denote the crack length after the dominant crack joins with the interfacial cracks. If the crack length before branching can be neglected (this assumption gives an error of δ less than 5%) then the crack lengths are approximately equal to

$$a = n\,b$$
$$a_{eff} = n(b + D_{avg}) \quad (B3)$$

when the dominant crack has intersected n aggregates.

For a given aggregate volume fraction, V_f

$$\frac{a_{eff}}{a} = \frac{b + D_{avg}}{b} = \frac{1}{1 - V_f} \quad (B4)$$

The opening separation δ is equated to the average opening contribution of the dominant crack as

$$\delta = \frac{S}{2a_{eff}} - \frac{S_0}{2a_{eff}} \quad (B5)$$

where $S = (2\pi\sigma/E)(1\text{-}\nu^2)(a_{eff})^2$ is the opening area of the crack faces, S_0 is that at the peak load, and the modified crack length a_{eff} is used in Equation (B5) to account for the dominant crack jumping effect. Therefore

$$\delta = \frac{\pi\sigma}{E}(1-\nu^2)\frac{a}{1-V_f} - \frac{\pi f_t}{E}\frac{(1-\nu^2)}{1-V_f}\frac{R_{max}^2}{a} \quad (B6)$$

Equation (B6), together with Equations (B1) and (B2) can be used to calculate the tension–softening curve. The final result has the form

$$\delta = \frac{(K_{Ic}^{eff})^2(1-\nu^2)}{E(1-V_f)f_t}\frac{1}{(\sigma/f_t)}[1 - (\sigma/f_t)^3] \quad (B7)$$